JACS
JOURNAL OF THE AMERICAN CHEMICAL SOCIETY

Article

pubs.acs.org/JACS

Conformational Order in Aggregates of Conjugated Polymers

Nicholas E. Jackson,[†] Kevin L. Kohlstedt,*[,†] Brett M. Savoie,[†] Monica Olvera de la Cruz,[†] George C. Schatz,[†] Lin X. Chen,[†,‡] and Mark A. Ratner*[,†]

[†]Department of Chemistry, Northwestern University, Evanston, Illinois 60208, United States

[‡]Chemical Sciences and Engineering Division, Argonne National Laboratory, Lemont, Illinois 60439, United States

Supporting Information

ABSTRACT: With the abundant variety and increasing chemical complexity of conjugated polymers proliferating the field of organic semiconductors, it has become increasingly important to correlate the polymer molecular structure with its mesoscale conformational and morphological attributes. For instance, it is unknown which combinations of chemical moieties and periodicities predictably produce mesoscale ordering. Interestingly, not all ordered morphologies result in efficient devices. In this work we have parametrized accurate classical force-fields and used these to compute the conformational and aggregation characteristics of single strands of common conjugated polymers. Molecular dynamics trajectories are shown to reproduce experimentally observed polymeric ordering, concluding that efficient organic photovoltaic devices span a range of polymer conformational classes, and suggesting that the solution-phase morphologies have far-reaching effects. Encouragingly, these simulations indicate that despite the wide-range of conformational classes present in successful devices, local molecular ordering, and not long-range crystallinity, appears to be the necessary requirement for efficient devices. Finally, we examine what makes a "good" solvent for conjugated polymers, concluding that dispersive π-electron solvent−polymer interactions, and not the electrostatic potential of the backbone interacting with the solvent, are what primarily determine a polymer's solubility in a particular solvent, and consequently its morphological characteristics.

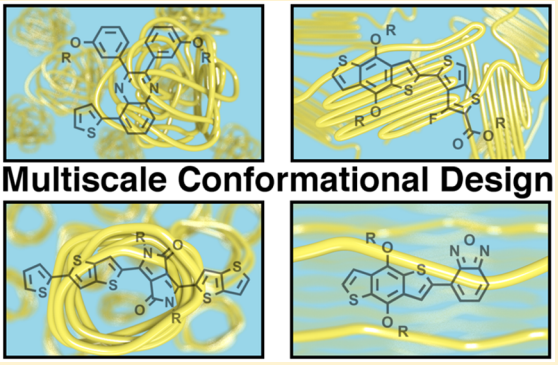

INTRODUCTION

Organic semiconductors have occupied the attention of the chemical sciences for three decades, with tailorable optoelectronic properties leading to a surge in fundamental and application-driven research. Design rules proposed by synthetic, experimental, and computational scientists have allowed for the rational control of local molecular structure to induce specific optoelectronic (optical gap,[1] oscillator strength,[2] energy level alignment,[3] reorganization energies[4]) and conformational (conformational locks,[5] backbone rigidity,[6] torsional alignment[7]) attributes. However, equivalent design rules for mesoscale (∼10−100 nm) conformational and morphological properties of conjugated polymers are not as prominent, despite the pervasive evidence that control over these length scales is critical to device performance. For example, in organic photovoltaics (OPV), the presence of locally ordered polymer aggregates has been shown to directly influence exciton dissociation,[8] charge transport,[9] and overall device performance.[10,11] The performances of organic field-effect transistors (OFET) also exhibit strong morphological dependencies, with polymer melts consisting of identical backbones displaying order of magnitude differences in charge carrier mobility depending on the processing conditions.[12,13] Similarly, polymer thermal conductivities show delicate associations with material crystallinity.[14,15] Given the highly complex, often kinetically trapped, nature of these morphologies, it is not surprising that few design rules[16−18] exist for how monomer molecular structure (∼1 nm) propagates into the mesoscale morphology (∼10−100 nm).

Ideally, one aims to deduce a polymer's mesoscale morphological characteristics and corresponding optoelectronic functionality from the molecular structure of the repeat unit, a task which is very complex. However, the prospect of rational control is favorable for conjugated polymers, since they encompass a broad spectrum of electrostatic and dispersion interactions that are absent in simpler plastics.[5] Conjugated polymers also possess variable rigidity and large off-axis chemical moieties that provide additional steric and solvation interactions that can be leveraged for control, although it is not fully understood how the interplay of these forces results in observed morphologies. In this work we demonstrate the power of fully atomistic simulations for predicting aggregation tendencies of conjugated polymers. The seminal coarse-grained simulations of Barbara and Rossky[19] showed that four polymer conformational classes—random coil, globule, toroid, and

Received: January 15, 2015
Published: April 28, 2015

DOI: 10.1021/jacs.5b00493
J. Am. Chem. Soc. 2015, 137, 6254−6262

rod—exist as simple functions of monomer properties, although subsequent work has yet to reveal an atomistic connection between molecular structure and these conformational classes. While significant work has studied the solution-phase conformations of P3HT and other first-generation conjugated polymers,[17,20−22] such rigorous attention to detail has not been directed toward the chemical variety of polymers appearing in the OPV and OFET literature, making the establishment of general trends across different conjugated structures difficult.

In this work we address three fundamental issues relating to polymer morphology prediction: accurate simulation of aggregates, determination of ideal polymer conformational properties, and the role of solvent in aggregate formation.

First, employing high-level quantum chemistry, we accurately parametrize a classical, OPLS-style[23] force-field for 15 low-band gap conjugated copolymers commonly studied in the OPV and OFET literature (Figure 1).[24−37] We outline how our

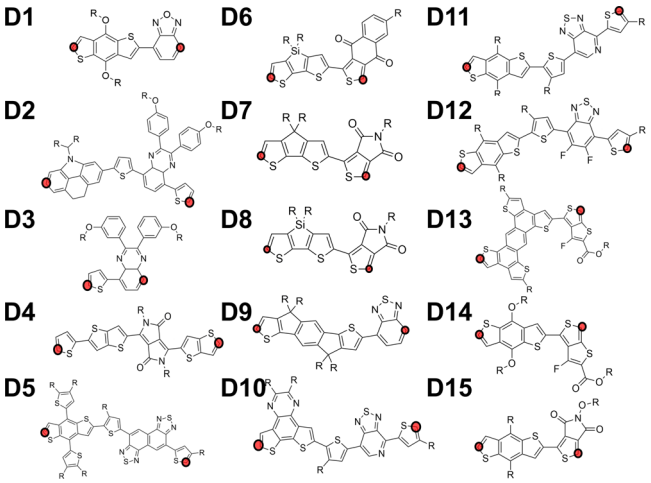

Figure 1. Structures of the repeat units for the polymers included in this study. Here R denotes an alkane side chain. The specific chemical structure of each R group is provided in the Supporting Information. The attachment points on each molecule are highlighted by red dots.

parametrization can be rapidly adapted to other materials, in-line with previous work,[38] allowing researchers to design a force-field for any arbitrary conjugated polymer.

Second, molecular dynamics (MD) simulations are utilized to assess the conformational classes and aggregation tendencies of our 15 chemically diverse polymer species. Through this process, we reproduce known coarse-grained polymer conformations with atomistic simulations, correlating molecular structure with canonical polymer conformational classes. Moreover, the order within and across classes of conformations is quantified using well-defined order parameters that provide a means of correlating mesoscopic order with monomer structure. These results are compared with experimental characterizations, when possible, and simple rational design rules are presented which relate molecular structure to mesoscale morphological tendencies. By comparing order parameters across molecular species, we conclude that successful polymers in organic semiconductor applications possess widely variable conformational and aggregation characteristics; there is no one ideal conformational class. Our analysis of polymer conformations reveals, in agreement with experimental X-ray characterization and related theoretical work,[9] that it is likely that only local molecular ordering (4−5 π-stacked chains), and not the commonly referenced long-range crystallinity, is a necessary condition for efficient charge and excitation transport. This result provides insight into the high performance of many inherently noncrystalline organic semiconductors, such as the OPV champion material PTB7.

Third, we stress that polymer morphology is highly tailorable with the correct processing conditions. To incorporate the processing aspect into our simulations, we examine the role of specific organic solvents, chloroform (CF) and chlorobenzene (CB), and how their interactions influence polymer conformations. It is shown that despite the diverse electrostatic potentials of the backbones in our polymer set, π-electron dispersion interactions are the dominant contribution to the solvation enthalpy, suggesting that the dispersion energy density of the solvent can be employed to alter polymer morphologies. Supporting this point, we show that the dispersion interaction energy grows with the size of the π-system, confirming that good solvents for these materials succeed by solvating the conjugated backbone, while the side-chain function is likely to sterically inhibit aggregate formation.

METHODS

Force-Field Parameterization. We utilize a combination of density functional and wave function-based electronic structure methods to accurately parametrize the empirical force field Optimized Potentials for Liquid Simulations (OPLS),[23] for 15 chemically diverse molecular structures to make the set OPLS-DA. All quantum-chemical calculations are performed using QCHEM 4.0.[39] A thorough description of parametrization procedures is provided in the Supporting Information, and in spirit is very similar to previous work on conjugated materials.[38]

Dihedrals. Each of the molecules in Figure 1 has one or more torsions between rings that are internal to the polymer unit (defined in Supporting Information). The torsional potentials associated with these angles were computed at 10° intervals. For each calculation, we constrain the dihedral angle between each unit and perform geometry optimization (B3LYP/6-31+G**) on all remaining degrees of freedom. These geometries are then used as inputs for RI-MP2/cc-pVTZ single-point energy calculations, and the resulting torsional potential energy surfaces are fit using the four-term OPLS dihedral potential. Standard OPLS parameters are taken for the torsional angles of the side-chains. We note that work has been performed suggesting a dependence of the torsional barrier height on chain length. In the case of polythiophene, the error in barrier height amounted to ∼1 kcal/mol difference between a dimer and a hexamer,[40] though it is unclear how much this difference is an artifact of a perfectly flat chain, as well as a bias of the self-interaction error of DFT. In our monomers, which are significantly larger than polythiophene, we expect these errors to be even smaller. Additionally, our focus on a smaller system size allows for a more accurate treatment of weak, noncovalent interactions with a high-level wave function method (RI-MP2), and thus should more accurately determine the positions and relative well depths of the torsional minima, which we believe should be more important to the morphological order than the torsional barrier height.

Geometries. To determine accurate intramolecular geometries, each polymer unit in Figure 1 is terminated with thiophenes on both sides to imitate the effect of being part of a conjugated backbone, as this will noticeably affect the backbone charge distribution. These structures are then optimized at the B3LYP/6-31+G** level of theory, and the internal equilibrium bond lengths and angles of each unit are added to the OPLS-DA force field. For the actual simulations, these terminating thiophenes are removed.

Stretching and Bending. Inter-ring harmonic stretching constants between conjugated units are determined by computing the potential energy surface of the bonded pair at varying intermolecular separations (B3LYP/6-31+G**), and fitting the resulting potential energy surface

DOI: 10.1021/jacs.5b00493
J. Am. Chem. Soc. 2015, 137, 6254−6262

to a harmonic potential, from which a harmonic force constant and equilibrium bond distance are extracted. All other stretching and bending parameters in the force-field are taken from common OPLS parameters for conjugated units and alkyl side-chains.

Atomic Partial Charges. It is necessary to parametrize the partial charges in these polymeric systems, as the existence of substantial electrostatic interactions between second and third row atoms is well-known. In previous work, we have observed the shortcomings of Mulliken charges due to their well-known instability with regard to basis set.[5] Atomic partial charges are calculated from the thiophene-terminated geometries (see Supporting Information for justification) using the "Charges from the Electrostatic Potential on a Grid" (ChelpG[41]) method for electrostatic potential fitting implemented in QCHEM 4.0, using the ground state electrostatic potential determined from a B3LYP/6-31+G** calculation.

van der Waals Interactions. All van der Waals interaction coefficients are taken from those defined for conjugated organic species in the original OPLS force-field.

Molecular Dynamics Simulations. *Conformational Class Determination: 30mer Simulations.* Using the OPLS-DA force-field, each of the polymers in the set was polymerized to be a linear chain of 30 repeat units (calculations using the reported molecular weights show that the lengths of polymers studied in the OPLS-DA set are between 30 and 250 repeat units). Each distinct MD trajectory begins with a random distribution of dihedral angles along the backbone, which is then energy minimized into a local minimum energy extended conformation. NVT simulations are performed with a background dielectric constant equivalent to chlorobenzene ($\varepsilon = 10$), a commonly used solvent. Simulated annealing is performed at 550 K for 1 ns to explore conformational space, followed by a linear cooling to 300 K over the course of 2 ns, settling into a local energy minimum. For each polymer species, five distinct trajectories are performed, totaling 15 ns for each polymer species. All MD simulations are performed using TINKER.[42] The conformational class of each polymer is determined by averaging the radii of gyration and dihedral distributions from the final conformations of all trajectories. In most cases, the conformations are sufficiently divergent that visual inspection is sufficient for categorization.

Aggregate Order Determination: Folded Strand Simulations. In the 30mer simulations, the extended polymer initial condition leads to many kinetically trapped, extended conformations where globules or aggregates cannot be accessed in the given simulation time. To explicitly sample the aggregates classes and their corresponding chain−chain π-stacking order, we artificially bias the initial simulation geometry to be in a singly folded conformation. To do this, each molecular structure in the OPLS-DA set is polymerized to a length corresponding to ∼150 nm. The oligomer is initially minimized in the extended conformation with a random distribution of dihedral angles. Following minimization, the oligomer is folded in half and minimized into the local, π-stacked minimum. This process occurs by defining a harmonic angle potential between the ends of the extended strand and its bisection point, and performing a minimization. Subsequently, this constraint is removed, and a regular minimization is performed to fall into the folded minimum. From this minimum, an NVT annealing run is performed for 2 ns at 550 K, followed by a linear cooling back down to 300 K over the course of 1 ns. Twenty trajectories are performed for each polymer species and the final geometric structure from each trajectory is used for order parameter analysis. While ideally the extent of these molecular dynamics simulations would be longer to more fully access global energy minima, sufficient divergence of conformational classes as a function of molecular structure can already be observed for our short trajectories, and often the conformational space of the aggregate becomes frozen upon aggregation, rendering longer trajectories as extremely inefficient explorations of phase space. Ideally, advanced sampling methods could be used in conjunction with Langevin dynamics to more fully sample phase space, but since our interest is primarily large trends in aggregated minima, these longer scale simulations of aggregate folding from an extended strand will be addressed in future studies.

Order Parameters and Contact Maps. The morphology of each polymer chain is classified according to the **Q**-tensor based on the Landau-de Gennes macroscopic order parameter,[43] averaged over all trajectories. The **Q**-tensor is defined as the second-order moment of the orientational distribution function f_ϕ (eq 1)

$$\mathbf{Q} = \int_{\mathbb{S}^2} \left(\mathbf{mm} - \frac{1}{3}\mathbf{I} \right) f_\varphi \, \mathrm{d}\mathbf{m} \tag{1}$$

where $\mathbf{m}$ is a measure of the space $\mathbb{S}^2$. For a given polymer, $\mathbf{m}$ corresponds to the unit vector $\hat{v}$, connecting the monomers along the backbone of the polymer. In the de Gennes formalism, the isotropic $\mathbf{Q}_0 = 1/3\mathbf{I}$ is subtracted, so $\mathbf{Q} = 0$ when polymers have no orientational order (i.e., isotropic). The eigenvalues (e_1, e_2, e_3) of $\mathbf{Q}$ provide information on the (bi/uni)-axial order of the individual polymeric units. An idealized rigid-rod polymer would have the largest positive eigenvalue e_1 equal to unity and the other two of the eigenvalues e_2, e_3 identically $-1/2$ ($\mathbf{Q}$ is traceless). The eigenvector b_1 of e_1 would provide the primary director for the polymer's orientation, which in the case of a perfectly rigid rod would correspond to the direction of the polymer backbone. The tensor itself is not amenable to visualization, but $\mathbf{Q}$ can be conceptually captured by correlating each polymer unit orientation as a contact map, where we visually represent the matrix $\mathbf{M}$ (eq 2).

$$\mathbf{M}_{ij} = \hat{v}_i \cdot \hat{v}_j \tag{2}$$

As an example of this type of analysis, Figure 2 presents the contact map and **Q**-tensor eigenvalues of a rigid-rod polymer, a singly folded

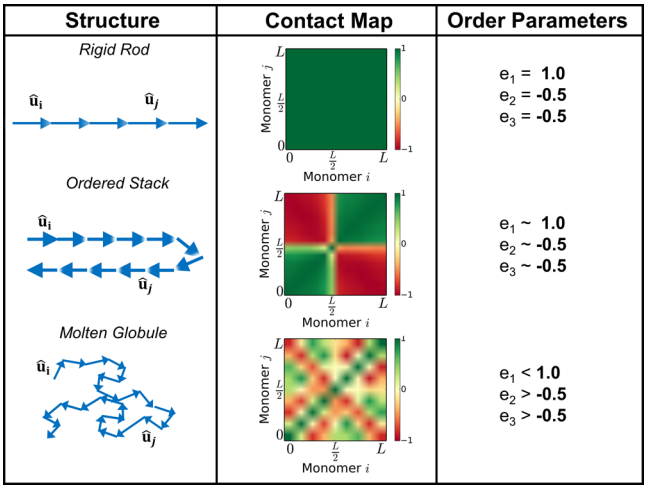

Figure 2. Structure, contact map, and **Q**-tensor eigenvalues of idealized rigid rod, ordered stack, and globule conformations.

rigid rod polymer, and a globular polymer. Note that for polymer strands exhibiting a single fold, antiparallel alignment (negative correlation−red) is observed between the first and second halves of the strand. In the folded strand simulations that follow, residual antiparallel correlations can be observed as a result of the initially folded geometry bias.

Tetramer Solvation Calculations. The OPLS-DA tetramers were solvated in a periodic cell of length 65 or 100 Å, depending on the DA unit size, with one of two chlorinated solvents, CB or CF. The density of solvent in the simulation cell was taken at 1 atm and 25 C, and for CB and CF it is 1.11 and 1.50 g/mL, respectively. Each solvation box is then locally minimized to remove bad contacts. The minimized cell was annealed for 700 ps at 550 K, before taking solvation measurements every 10 ps for another 500 ps at 300 K; the electrostatic, E_{charge}, van der Waals, E_{disp}, and total potential energy, $E_{\mathrm{sys}} = E_{\mathrm{charge}} + E_{\mathrm{disp}}$ were calculated from each snapshot, as well as the radius of gyration (R_g).

The enthalpy of mixing ΔH_m for each polymer solvent system was calculated from the intermolecular interactions between the tetramer

DOI: 10.1021/jacs.5b00493
J. Am. Chem. Soc. 2015, 137, 6254−6262

and the solvent shell of the conformationally averaged trajectories. From each trajectory, the solvent cohesive energy density (ε_{solv}) and polymer self-interaction energies (E_{DA}) are also calculated, taking into account only the E_{charge} and E_{disp} components of the energy. We write the solvation energy density for each polymer as

$$\frac{\Delta H_m}{V_{DA}} = \frac{E_{sys} - \varepsilon_{solv} V_{box} - E_{DA}}{V_{DA}} \quad (1)$$

where V_{DA} and V_{box} are volumes of the swollen tetramer and box, respectively.

RESULTS

Canonical Conformational Classes from 30mer Trajectories. MD simulations of 30mers of each polymer species are performed to assess the conformational class of each polymer. To account for the existence of specific $\pi-\pi$ interactions in these materials, we have adjusted our conformational class definitions relative to those of Rossky to reflect the detail of the atomistic simulations (Figure 3): rod/ideal-chain,

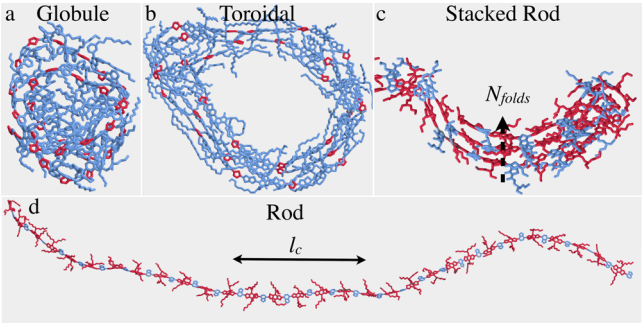

Figure 3. Four mesoscale conformations observed in 30mer trajectories: (a) globule, (b) toroid, (c) stacked rod, and (d) rod. Red entities represent the electron "donor" block of the copolymer backbone, while blue represents the electron "acceptor" block. In panel c, N_{folds}, is the number of folded layers in the stacked rod. In d, l_c is the conjugated length of the polymer.

globule, toroid, and stacked rod. The differentiation between globule and stacked rod is vital, as these two aggregate types possess vastly different optoelectronic properties due to different dihedral distributions and π-stacking order. Additionally, we characterize the dihedral order of each, using the classification "twisted" to define low dihedral barriers and nonplanar dihedral minima, and "planar" to define high dihedral barriers and planar minima.

It is clearly observed (Supporting Information Figure S1–S15) that the resultant conformations from the OPLS-DA set span the four canonical conformational classes previously defined. Specifically, we find that polymers with linear conjugated backbones and small geometric components orthogonal to the direction of the backbone (D1, D4, D9, D12, D13, D14, D15) possess the greatest ability to form the ordered classes of rod/ideal-chain, stacked rod, and toroid (see Supporting Information). Conversely, polymers with nonlinear conjugated backbones and/or cramped alkyl side-chain interactions (D2, D3, D5, D7, D8, D10, D11) are more prone to the disordered globule state. Polymers that are intermediate between these two extremes of linearity (D7, D8, D11) exhibit a mixture of ordered and disordered conformational classes. These results support the concept that backbone linearity is fundamental to obtaining ordered conformational classes, and consequently crystalline materials. However, it is important to note that side-chain choice is a tunable parameter that can likely seriously affect extended polymer conformations. Previous work has shown that side-chain density and placement in P3HT alters the backbone conformations via entropic (excluded volume) and dispersion interactions.[21,44] Consequently, a conjugated backbone's linearity is only an initial guess for its ability to π-stack and form ordered conformational classes.

While backbone linearity is one fundamental determinant of ordered conformational class formation, the ability of these molecules to form π-stacks can be influenced by the dihedral angle distribution of the polymer, which incorporates both the monomer–monomer torsional potential, as well as side-chain/side-chain interactions. The dihedral distributions of the 30mer trajectories were analyzed to quantify the relative impact of dihedral distortion on the observed conformations (Supporting Information Figure S1–S15). From these distributions it is clear that the computed monomer–monomer RI-MP2 torsional potential serves as a reasonable approximation to the dihedral distributions obtained from MD trajectories. However, in a number of cases the relative population of particular wells does not correspond to that predicted from the RI-MP2 dihedral partition function (D2, D3, D4, D5, D9, D11, D12). Additionally, polymers with attainable planar dihedral angles are often observed to have little population at planar dihedral angles, and significantly more at a 30°–60° deviation from the minimum. This result is indicative of strong side-chain interactions in the polymer globule. Consequently, the torsional potential computed from electronic structure methods is often not a reliable predictor of torsional potentials in the aggregate, particularly for materials that do not already possess strong ordering tendencies.

The relationship between the ordering tendency of the aggregate and the RI-MP2 dihedral potential can be directly analyzed from the 30mer trajectories. The dihedral potential is fundamentally related to the conjugation length of the polymer, and the ability of a particular conformational class to π-stack requires coordination of multiple conjugated units. From a comparison of all polymers (Supporting Information Figure S1–S15), it is observed that while polymers with planar dihedral minima (D1, D4, D7, D8, D9, D10, D12, D15) are often planar (D1, D4, D9, D15), notable exceptions occur (D7, D8, D10, D12). In the cases of D7, D8, D10, and D12, all of these polymers possess nonlinear backbones, and this is likely the reason that their 30mer trajectories do not all result in highly ordered conformational classes. Contrastingly, linear backbones with nonplanar dihedral minima tend to form stacked rods that possess significant torsional disorder, resulting in twisted, stacked rod conformations.

We briefly note that the knowledge gained from conformational class determination for these polymers (See Supporting Information Figure S1–S15) can have a great impact on spectroscopic analysis and computational rational design. Recent spectroscopic work has analyzed the role of solution-phase aggregation on ultrafast spectroscopic quantities in great detail,[20,45−48] and an atomistic picture of chain conformations is fundamental to interpreting spectroscopic data.[49] The fact that classical force-fields can be rapidly adapted to any conjugated polymer provides an exciting avenue that can complement current spectroscopic work. On the rational design front, one could use high-level computational methods to correlate molecular descriptors with conformational class, and incorpo-

DOI: 10.1021/jacs.5b00493
J. Am. Chem. Soc. 2015, 137, 6254–6262

rate the polymer mesoscale into a computational rational design process.[50,51]

Quantifying Order in the Polymer Aggregate. While the previous 30mer calculations showcase a polymer's conformational tendencies, it is necessary from an optoelectronic viewpoint to quantify the fine detail regarding polymeric ordering present in the aggregated state. To this end, foundational work by Spano has formulated this ordering in terms of simple spectroscopic observables.[52] Aggregate fluorescence studies by various groups have also provided much experimental insight into aggregate order.[53−55] In the film, and often in dilute solutions,[46] polymer strands will be aggregated, and thus we aim to elucidate the precise aggregate order for an arbitrary polymer with atomistic detail. To this end, we examine artificially folded (aggregated) single strands of each polymer in the OPLS-DA set, and compute order parameters that provide insight into the backbone ordering in the aggregated state.

While a variety of molecular structures have been parametrized and studied in this work, we have chosen three experimentally well-characterized molecular structures (Figure 4) on which to demonstrate the power of this approach to

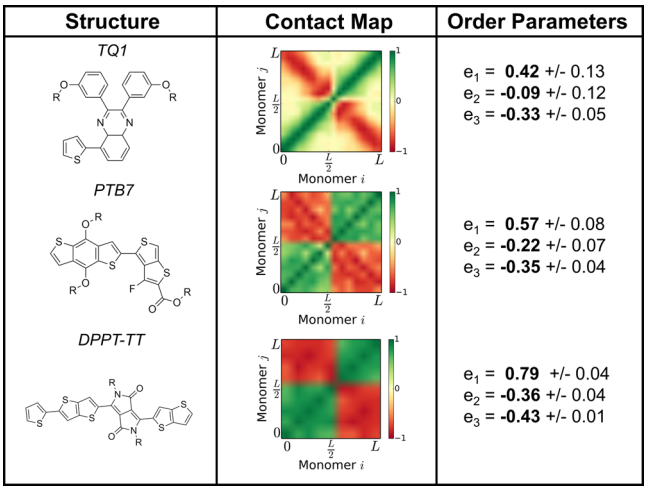

Figure 4. Structure, contact map, and **Q**-tensor eigenvalues of TQ1 (D3), PTB7 (D14), and DPPT-TT (D4).

determining polymer order, TQ1 (D3), DPPT-TT (D4), and PTB7 (D14). These three structures span a wide range of polymeric order, and thus provide an experimental benchmark to compare simulations against. For an analysis of other members of the OPLS-DA set, we direct the interested reader to the Supporting Information.

Disordered TQ1. Analysis begins with TQ1, one of the most disordered materials present in OPLS-DA. All 30mer trajectories for TQ1 resulted in the disordered globule conformation. When TQ1 is folded into the aggregated state, annealed, and analyzed using the de Gennes formalism, it becomes readily apparent that TQ1 exhibits no strong ordering tendencies as evidenced by the lack of correlation in the contact map beyond nearest neighbors. Additionally, **Q**-tensor eigenvalues (e_1 = 0.42, e_2 = −0.09, e_3 = −0.33) show little uniaxial alignment providing further evidence that there is no dominant director present in the system. The dihedral distribution derived from molecular dynamics trajectories is also highly nonplanar, as expected from the computed torsional potentials.

Experimental characterization demonstrates that TQ1 forms little long-range π-system order in either film or solution. Powder X-ray diffraction measurements show clear peaks at 25.1 and 4.33 Å, indicating regular spacing between π-conjugated main chains and loosely packed alkyl chains, respectively; the fact that the spacing between π-conjugated main chains is so large suggests significant torsional disorder, and little-to-no π-stacking. This characteristic π-system disorder is supported by the visible absorption spectrum of both the solution and the film.[26,56] The presence of vibronic structure or spectral shifts in the film and solution absorption spectra are indicative of π-ordering and backbone planarization, respectively. Polymers that are strongly ordered in solution exhibit a negligible red-shift when cast as a film, and possess vibronic fine structure in both the solution and film absorption spectra. In solution TQ1 exhibits a Gaussian absorption that is significantly blue-shifted from the film absorption,[26] and depositing the material into the film planarizes the backbone, redshifting the absorption. The authors note that heating the solution to 100 °C results in a blue shift of the absorption, indicating the dispersal solution-phase aggregates. However, the distinct lack of vibronic structure indicates the absence of torsional ordering in the solution aggregate. Even in film, TQ1's absorption spectrum does not demonstrate the vibronic fine structure that is characteristic of many conjugated polymers, suggesting that the π-system is highly disordered. The π -system disorder of TQ1 can be correlated with the nonlinear geometric shape of the monomer molecular structure, along with the nonplanar dihedral minima.

Crystalline DPPT-TT. Having had success describing the disordered structure of TQ1, we now examine a highly ordered structure, DPPT-TT. Experimentally, diketopyrrolopyrrole-based polymers are known for their strong crystallinity, high OFET mobilities, and long-range order in films of these materials.[57] This specific flavor of DPPT-TT polymer[27] also demonstrates strong ordering and a well-defined π-stacking peak at 3.8 Å, as revealed through X-ray characterization.[12] Spectroscopically, this material has nearly identical experimental solution and film absorption spectra, possessing well-defined vibronic structure in both solution and film, as well as a negligible redshift of the absorption edge after being deposited into the film, all of which indicate a highly ordered structure in both solution and film.

Folded strand simulations of DPPT-TT suggest it to be one of the most ordered polymers in the OPLS-DA set, demonstrating only rod/ideal-chain or stacked rod classes in the 30mer calculations. In computations of the folded strand, DPPT-TT's **Q**-tensor eigenvalues suggest a highly ordered system (e_1 = 0.75, e_2 = −0.34, e_3 = −0.41), which can be visually represented through the contact map showing strong correlations beyond nearest neighbors (Figure 4). The torsional potential of DPPT-TT has deep planar minima and a large torsional barrier, which can be attributed to the significant quinoidal character of DPPT-TT, as well as the presence of nontraditional intramolecular hydrogen bonds.[5] The linearity of the DPPT-TT backbone also appears to be conducive to forming an ordered structure.

Locally Ordered, Noncrystalline PTB7. The simulation techniques described previously have properly characterized two extremes of the order spectrum for conjugated polymers, highly amorphous, and highly crystalline. We now extend the simulations to, for the first time, examine the conformational and aggregation properties of PTB7 using atomistic MD. It is

DOI: 10.1021/jacs.5b00493
J. Am. Chem. Soc. 2015, 137, 6254−6262

well-known that PTB7 is not highly crystalline in bulk-heterojunction (BHJ) blends and neat films, though it still exhibits record device efficiencies when incorporated into OPV.

Experimentally, PTB7 is well characterized. X-ray diffraction performed on neat films showed two diffraction peaks, one at 3.8−4.0 Å (π-stacking) and the other at 28−31 Å corresponding to the spacing between coplanar alkyl chains.[58] Other work has described the content of PTB7 domains in the active layer to be ∼20% crystalline, supporting the existence of a high fraction of amorphous polymer.[59] Scherrer analysis of the coherence lengths of π-stacked domains yielded an average coherence length of ∼4−5 stacked chains for PTB7, as opposed to ∼16 stacks for P3HT, further underscoring the mixed amorphous/crystalline propensities of PTB7.

The linear absorption spectrum of PTB7 exhibits identifiable, though not well-defined, vibronic structure in its solution spectrum, as well as in its thin film spectrum, with a negligible redshift in going from solution to film. This is indicative of ordered aggregation occurring in both the solution and the film. Other studies of materials closely related to PTB7 have demonstrated that the solution-phase spectrum significantly blueshifts and loses vibronic structure upon heating.[60] Changing the aggregate character in PTB7 also intimately affects charge generation dynamics, with more ordered aggregates exhibiting a larger branching ratio of charge separated to charge transfer states.[60]

Simulations of PTB7 reveal a system which is intermediate between the highly disordered TQ1, and the highly ordered DPPT-TT. The results of the 30mer simulations show a system which sometimes adopts stacked rods, and sometimes globules. This is consistent with previous studies showing subtle side-chain variations affecting the nature of the aggregate.[60] **Q**-tensor eigenvalues of ($e_1 = 0.57$, $e_2 = -0.22$, $e_3 = -0.35$) suggest a state of intermediate order, which is additionally supported by the well-defined contact map of the folded strand simulations. The contact map correlations are weaker than those in DPPT-TT, but clearly much stronger than in the case of TQ1.

Are Rigid π-Systems a Requirement for Efficient Devices? Conventional rational design for conjugated polymeric materials typically revolves around the following concept: large, rigid π systems and planar dihedral minima with large torsional barriers will enhance π-stacking and increase crystallinity. However, given the above analysis of TQ1, DPPT-TT, and PTB7, it is clear that high-performance conjugated polymers cover a variety of conformational classes. Note that we are not referring to the BHJ cell, only the innate conformational characteristics of the polymer species itself. Indeed, the highest performing OPV material to date, PTB7, is not highly ordered over long length scales, and only maintains order over the scale of ∼4 π-stacks. In support of this point, Supporting Information Figure S1−S15 list the value of the largest positive order parameter computed for each material in our polymer set, as well as the optimized OPV BHJ power conversion efficiency (PCE) for each. Despite the variations in polymer ordering, all polymers, crystalline or amorphous, possess PCE well over 5%. Given this knowledge, the synthetic strategy of rigid conjugated polymer backbones does not seem immediately necessary, although the benefits of planarity for intramolecular charge transport are obvious, given that the intermonomer coupling is a function of the dihedral angle.[61]

For BHJ, it is possible that the ideal polymer would be flexible enough to pack efficiently and explore phase space, yet rigid and ordered enough to possess good charge transport over short length scales. More rigid polymers would favor transport but frustrate packing,[62] while completely amorphous polymers would pack well but poorly transport charge, in agreement with recent theoretical work by Troisi demonstrating that the mechanism of charge transport changes from intramolecular to intermolecular as a function of backbone rigidity.[63] Perhaps the best compromise between these extremes is an amorphous polymer with a planar backbone, as was recently reported as achieving high carrier mobilities.[64] It is telling that the most successful OPV polymers are not remarkable OFET materials, which favor highly crystalline structures. Similar arguments have been made in the field of ionic transport polymers.[62] Consequently, rigid backbones might be better for OFETs, where charge transport must occur over longer length scales. In OPVs, backbone flexibility might more successfully accommodate fullerene domains, since charge transport must navigate the convoluted bicontinuous domains of the BHJ.

With a typical length scale of π-stacking correlations of approximately four chains, PTB7 might be a good intermediate point between the rigid and flexible charge transport regimes. Consequently, utilizing localized order in a sea of disorder could be an excellent design strategy for circumventing many of the problems associated with disordered organic semiconductors. This argument has been put forth in a similar context, using regularly localized molecular orbitals to achieve high charge mobilities in a noncrystalline film.[18]

The role that processing plays in organic semiconductor devices cannot be overstated. It has been clearly shown that record charge carrier mobilities can be achieved by using sophisticated processing techniques to align polymer strands.[65] Aggregate formation through the intentional use of poor solvents has also induced large increases in mobilities.[66] Indeed, innumerable advances in OPV device performance have come as a result of processing additives and annealing techniques.[67,68] As a result, it is evident that most polymers can be processed into a wide variety of morphologies and this largely explains how polymers with such disparate morphological features can produce high-performing devices. Consequently, the simulations performed here only represent the conformational tendencies and preferences of a given material, though the actual morphologies can be significantly altered with the correct processing techniques.

Polymer−Solvent Interactions. The fundamental role solvent plays in dictating polymer conformation has been known since the early work of Flory.[69] Since the previous calculations did not include explicit solvent interactions, they represent an approximation to the conformations a polymer would take in solvent. To elucidate the effects of solvent on conjugated polymer conformations, we have performed explicit solvent simulations of tetramers of the OPLS-DA set in two common solvents, chloroform (CF) and chlorobenzene (CB).

To understand the role of solvent in dictating conformations, it is first necessary to understand whether the dominant solvating interaction is predominantly electrostatic or dispersive in nature.[70−72] By determining if electrostatic or dispersive interactions are dominant, one can identify the ability to shift the solution-phase conformations of polymers by rationally varying solvent quality. To provide insight into solvation effects, we plot the solvation enthalpy density (SED = $\Delta H_t/V_{DA}$) versus both the dispersion and electrostatic components of the interaction energy, for all members of the OPLS-DA set in both CB and CF (Figure 5). Figure 5 clearly demonstrates that the SED exhibits a strong correlation with the dispersion energy

DOI: 10.1021/jacs.5b00493
J. Am. Chem. Soc. 2015, 137, 6254−6262

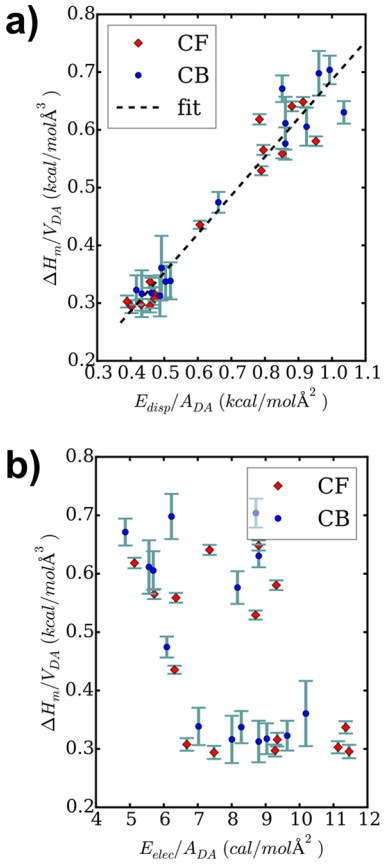

Figure 5. Solvation enthalpy density versus dispersion interaction energy of all polymers in CF and CB explicit solvent. (a) The dispersion interaction collapses the SED of the polymers onto a line (dashed). (b) Conversely, the electrostatic energy shows no correlation with the SED.

component, and no correlation with the electrostatic energy component. This result is encouraging for the rational control of polymer conformations, as it reveals that the precise nature of the electrostatic potential of the backbone is largely irrelevant for morphological control; the dispersion component of the energy is significantly more important. Consequently, if one is trying to control the quality of the solvent to influence conformations, one can, as a first approximation, only focus on the dispersion parameter of the solvent. Such interaction specific solvent control is the essence of Hansen's approach to solubility.[72,73]

While dispersion energy is the dominant component of the interaction between polymer and solvent, its exact origin is not clear, as both solvent−backbone and solvent−side-chain interactions exist. By examining the SED for all polymers in both CF and CB (Figure 6), it is clear that the polymers with

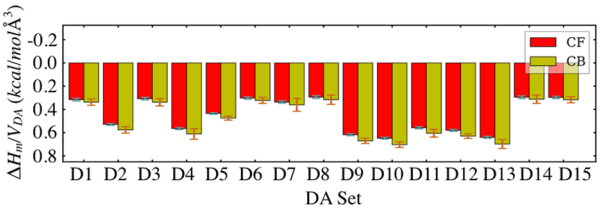

Figure 6. Solvation energy densities for all OPLS-DA polymers in both CF and CB.

the most π-electrons per repeat unit exhibit the largest SED. This result suggests that solubility and conformational control are primarily induced by backbone-solvent interactions; a conclusion which makes intuitive sense, as sp^3 alkyl carbons generally have very weak interactions, while the π-systems carry strong dispersion interactions. This argument is additionally supported by the fact that experimentally chlorinated solvents are always good solvents for conjugated polymers; a fact which can be attributed to CF, CB, and 1,2-dichlorobenzene's (DCB) chlorine atoms (which carry a larger van der Waals coefficient than carbon) and CB and DCB's aromatic structure. In final agreement with this point is the fact that in Figure 6, CB is a better solvent than CF for the majority of materials studied, suggesting that the flat π-system of CB can more effectively maximize dispersive interactions than the tetrahedral CF.

Regarding the role of side chains, it is likely that their role is primarily to entropically penalize aggregate formation by sterically interrupting interactions between π-systems. While we do not possess definitive evidence at this time, we suspect that solvation has little to do with advantageous side-chain/solvent interactions. This point is additionally supported by the common experimental observation that two alkyl chains, one branched and one linear, with the same number of carbons, will exhibit drastically different solubility, with the branched group being more soluble. Since a branched chain and a linear chain of the same length will possess nearly identical surface areas for solvent interactions, this point additionally supports the absence of advantageous side-chain/solvent interactions.

With this in mind, one can consider the ability to control polymer conformations via solvent choice. Conventionally, one expects bad solvents to cause a decrease in the radius of gyration. Even in simulations as small as tetramers in two "good" solvents, the radii of gyration of our polymer set (Supporting Information Figure S16) are typically smaller in CF than in CB, especially for longer tetramers (D2/D5) in agreement with CB often being a better solvent for these materials. With this in mind, one can work to control how aggregated a polymer is in solution prior to its deposition. If the goal is to deposit long, extended strands into the film, one should choose a solvent that maximizes dispersive interactions. If one would like to aggregate the solvent as much as possible prior to deposition, a solvent should be chosen which has a lower dispersive interaction density, causing the radius of gyration to shrink, completely analogously to solvent quality in Flory's formulation. We hypothesize that the dispersive interactions necessary for solubilizing conjugated polymers might place an upper limit on the π-electron density one may have in a repeat unit, as the only solvents capable of matching that dispersion energy density will be π-systems themselves, which at some size cease to be liquids.

CONCLUSION

Using high-level quantum-chemical computation, we have parametrized an OPLS-style classical force-field for a set of 15 diverse polymer molecular structures, and used it to study a variety of conjugated polymer morphological attributes. By analyzing the conformational classes of our polymer set using MD simulations, we present simple design rules relating a polymer's molecular structure to its mesoscale conformational class. We compare our computational results to experimental results for three paradigmatic conjugated polymers, concluding that only local polymer ordering, and not long-range crystallinity, is a necessary requirement for efficient organic

DOI: 10.1021/jacs.5b00493
J. Am. Chem. Soc. 2015, 137, 6254−6262

semiconductor devices. Supporting this point, it is demonstrated that successful OPV BHJ polymers span a wide variety of conformational classes, indicating the overriding importance of processing in these devices.

Molecular dynamics simulations are performed to determine the attributes of a "good" solvent for conjugated polymers. We conclude that dispersive interactions, namely the size of the π-electron system, play the dominant role in determining the solvation energy of a polymer, with the electrostatic potential of our diverse polymer backbones playing a far lesser role. We suggest that the primary role of solubilizing side chains is to entropically penalize aggregate formation by interrupting $\pi-\pi$ interactions between chains.

■ ASSOCIATED CONTENT

Supporting Information

Force-field parametrization details. Stretching constants, dihedral potentials, molecular geometries, atomic partial charges and example input files needed for force-field usage. Dihedral potentials computed at RI-MP2, B3LYP, and omegaB97x levels of theory. Order parameters, contact maps, and experimental characterization for all materials in the OPLS-DA polymer set. Tetramer solvation plot of the radius of gyration. The Supporting Information is available free of charge on the ACS Publications website at DOI: 10.1021/jacs.5b00493.

■ AUTHOR INFORMATION

Corresponding Authors

*kkohlstedt@northwestern.edu
*ratner@northwestern.edu

Notes

The authors declare no competing financial interest.

■ ACKNOWLEDGMENTS

We thank the U.S. DOE-BES Argonne-Northwestern Solar Energy Research Center (ANSER), an Energy Frontier Research Center (Award DE-SC0001059) for funding this project. N.E.J. thanks the NSF for the award of a Graduate Research Fellowship (NSF DGE-0824162). K.L.K. acknowledges support from AFOSR MURI Grant FA9550-11-1-0275.

■ REFERENCES

(1) Roncali, J. *Macromol. Rapid Commun.* **2007**, *28*, 1761.
(2) Grimm, B.; Risko, C.; Azoulay, J. D.; Brédas, J.-L.; Bazan, G. C. *Chem. Sci.* **2013**, *4*, 1807.
(3) Ohkita, H.; Cook, S.; Astuti, Y.; Duffy, W.; Tierney, S.; Zhang, W.; Heeney, M.; McCulloch, I.; Nelson, J.; Bradley, D. D. C.; Durrant, J. R. *J. Am. Chem. Soc.* **2008**, *130*, 3030.
(4) Hutchison, G. R.; Ratner, M. A.; Marks, T. J. *J. Am. Chem. Soc.* **2005**, *127*, 2339.
(5) Jackson, N. E.; Savoie, B. M.; Kohlstedt, K. L.; Olvera de la Cruz, M.; Schatz, G. C.; Chen, L. X.; Ratner, M. A. *J. Am. Chem. Soc.* **2013**, *135*, 10475.
(6) Wijsboom, Y. H.; Patra, A.; Zade, S. S.; Sheynin, Y.; Li, M.; Shimon, L. J. W.; Bendikov, M. *Andew. Chem., Int. Ed.* **2009**, *48*, 5443.
(7) Kanimozhi, C.; Naik, M.; Yaacobi-Gross, N.; Burnett, E. K.; Briseno, A. L.; Anthopoulos, T. D.; Patil, S. *J. Phys. Chem. C* **2014**, *118*, 11536.
(8) Gao, J.; Niles, E. T.; Grey, J. K. *J. Phys. Chem. Lett.* **2013**, 2953.
(9) Rühle, V.; Kirkpatrick, J.; Andrienko, D. *J. Chem. Phys.* **2010**, *132*, 134103.
(10) Noriega, R.; Rivnay, J.; Vandewal, K.; Koch, F. P. V.; Stingelin, N.; Smith, P.; Toney, M. F.; Salleo, A. *Nat. Mater.* **2013**, *12*, 1038.
(11) Kline, R. J.; McGehee, M. D.; Kadnikova, E. N.; Liu, J.; Fréchet, J. M. J.; Toney, M. F. *Macromolecules* **2005**, *38*, 3312.
(12) Chen, Z.; Lee, M. J.; Shahid Ashraf, R.; Gu, Y.; Albert-Seifried, S.; Meedom Nielsen, M.; Schroeder, B.; Anthopoulos, T. D.; Heeney, M.; McCulloch, I.; Sirringhaus, H. *Adv. Mater.* **2012**, *24*, 647.
(13) O'Connor, B. T.; Reid, O. G.; Zhang, X.; Kline, R. J.; Richter, L. J.; Gundlach, D. J.; DeLongchamp, D. M.; Toney, M. F.; Kopidakis, N.; Rumbles, G. *Adv. Funct. Mater.* **2014**, *24*, 3422.
(14) Shen, S.; Henry, A.; Tong, J.; Zheng, R.; Chen, G. *Nat. Nano.* **2010**, *5*, 251.
(15) Wang, D.; Shi, W.; Chen, J.; Xi, J.; Shuai, Z. *Phys. Chem. Chem. Phys.* **2012**, *14*, 16505.
(16) Bounos, G.; Ghosh, S.; Lee, A. K.; Plunkett, K. N.; DuBay, K. H.; Bolinger, J. C.; Zhang, R.; Friesner, R. A.; Nuckolls, C.; Reichman, D. R.; Barbara, P. F. *J. Am. Chem. Soc.* **2011**, *133*, 10155.
(17) Traub, M. C.; DuBay, K. H.; Ingle, S. E.; Zhu, X.; Plunkett, K. N.; Reichman, D. R.; Vanden Bout, D. A. *J. Phys. Chem. Lett.* **2013**, *4*, 2520.
(18) Terao, J.; Wadahama, A.; Matono, A.; Tada, T.; Watanabe, S.; Seki, S.; Fujihara, T.; Tsuji, Y. *Nat. Commun.* **2013**, *4*, 1.
(19) Hu, D.; Yu, J.; Wong, K.; Bagchi, B.; Rossky, P. J.; Barbara, P. F. *Nature* **2000**, *405*, 1030.
(20) Nguyen, T.-Q.; Doan, V.; Schwartz, B. J. *J. Chem. Phys.* **1999**, *110*, 4068.
(21) Hu, Z.; Adachi, T.; Lee, Y.-G.; Haws, R. T.; Hanson, B.; Ono, R. J.; Bielawski, C. W.; Ganesan, V.; Rossky, P. J.; Vanden Bout, D. A. *ChemPhysChem* **2013**, *14*, 4143.
(22) Adachi, T.; Brazard, J.; Ono, R. J.; Hanson, B.; Traub, M. C.; Wu, Z.-Q.; Li, Z.; Bolinger, J. C.; Ganesan, V.; Bielawski, C. W.; Vanden Bout, D. A.; Barbara, P. F. *J. Phys. Chem. Lett.* **2011**, *2*, 1400.
(23) Jorgensen, W. L.; Maxwell, D. S.; Tirado-Rives, J. *J. Am. Chem. Soc.* **1996**, *118*, 11225.
(24) Nie, W.; MacNeill, C. M.; Li, Y.; Noftle, R. E.; Carroll, D. L.; Coffin, R. C. *Macromol. Rapid Commun.* **2011**, *32*, 1163.
(25) He, Z.; Zhang, C.; Xu, X.; Zhang, L.; Huang, L.; Chen, J.; Wu, H.; Cao, Y. *Adv. Mater.* **2011**, *23*, 3086.
(26) Wang, E.; Hou, L.; Wang, Z.; Hellström, S.; Zhang, F.; Inganäs, O.; Andersson, M. R. *Adv. Mater.* **2010**, *22*, 5240.
(27) Bronstein, H.; Chen, Z.; Ashraf, R. S.; Zhang, W.; Du, J.; Durrant, J. R.; Shakya Tuladhar, P.; Song, K.; Watkins, S. E.; Geerts, Y.; Wienk, M. M.; Janssen, R. A. J.; Anthopoulos, T.; Sirringhaus, H.; Heeney, M.; McCulloch, I. *J. Am. Chem. Soc.* **2011**, *133*, 3272.
(28) Wang, M.; Hu, X.; Liu, P.; Li, W.; Gong, X.; Huang, F.; Cao, Y. *J. Am. Chem. Soc.* **2011**, *133*, 9638.
(29) Cui, C.; Fan, X.; Zhang, M.; Zhang, J.; Min, J.; Li, Y. *Chem. Commun.* **2011**, *47*, 11345.
(30) Li, Z.; Tsang, S.-W.; Du, X.; Scoles, L.; Robertson, G.; Zhang, Y.; Toll, F.; Tao, Y.; Lu, J.; Ding, J. *Adv. Funct. Mater.* **2011**, *21*, 3331.
(31) Chu, T.-Y.; Lu, J.; Beaupré, S.; Zhang, Y.; Pouliot, J.-R.; Wakim, S.; Zhou, J.; Leclerc, M.; Li, Z.; Ding, J.; Tao, Y. *J. Am. Chem. Soc.* **2011**, *133*, 4250.
(32) Chen, Y.-C.; Yu, C.-Y.; Fan, Y.-L.; Hung, L.-I.; Chen, C.-P.; Ting, C. *Chem. Commun.* **2010**, *46*, 6503.
(33) Zhou, H.; Yang, L.; Price, S. C.; Knight, K. J.; You, W. *Andew. Chem., Int. Ed.* **2010**, *49*, 7992.
(34) Zhou, H.; Yang, L.; Stuart, A. C.; Price, S. C.; Liu, S.; You, W. *Andew. Chem., Int. Ed.* **2011**, *50*, 2995.
(35) He, F.; Wang, W.; Chen, W.; Xu, T.; Darling, S. B.; Strzalka, J.; Liu, Y.; Yu, L. *J. Am. Chem. Soc.* **2011**, *133*, 3284.
(36) Liang, Y.; Xu, Z.; Xia, J.; Tsai, S.-T.; Wu, Y.; Li, G.; Ray, C.; Yu, L. *Adv. Mater.* **2010**, *22*, E135.
(37) Piliego, C.; Holcombe, T. W.; Douglas, J. D.; Woo, C. H.; Beaujuge, P. M.; Fréchet, J. M. J. *J. Am. Chem. Soc.* **2010**, *132*, 7595.
(38) DuBay, K. H.; Hall, M. L.; Hughes, T. F.; Wu, C.; Reichman, D. R.; Friesner, R. A. *J. Chem. Theory Comput.* **2012**, *8*, 4556.
(39) Shao, Y.; Molnar, L. F.; Jung, Y.; Kussmann, J.; Ochsenfeld, C.; Brown, S. T.; Gilbert, A. T. B.; Slipchenko, L. V.; Levchenko, S. V.; O'Neill, D. P.; D, R. A., Jr.; Lochan, R. C.; Wang, T.; Beran, G. J. O.; Besley, N. A.; Herbert, J. M.; Lin, C. Y.; Voorhis, T. V.; Chien, S. H.;

DOI: 10.1021/jacs.5b00493
J. Am. Chem. Soc. 2015, 137, 6254−6262

Sodt, A.; Steele, R. P.; Rassolov, V. A.; Maslen, P. E.; Korambath, P. P.; Adamson, R. D.; Austin, B.; Baker, J.; Byrd, E. F. C.; Dachsel, H.; Doerksen, R. J.; Dreuw, A.; Dunietz, B. D.; Dutoi, A. D.; Furlani, T. R.; Gwaltney, S. R.; Heyden, A.; Hirata, S.; Hsu, C.-P.; Kedziora, G.; Khalliulin, R. Z.; Klunzinger, P.; Lee, A. M.; Lee, M. S.; Liang, W.; Lotan, I.; Nair, N.; Peters, B.; Proynov, E. I.; Pieniazek, P. A.; Rhee, Y. M.; Ritchie, J.; Rosta, E.; Sherrill, C. D.; Simmonett, A. C.; Subotnik, J. E.; Iii, H. L. W.; Zhang, W.; Bell, A. T.; Chakraborty, A. K.; Chipman, D. M.; Keil, F. J.; Warshel, A.; Hehre, W. J.; Iii, H. F. S.; Kong, J.; Krylov, A. I.; Gill, P. M. W.; Head-Gordon, M. *Phys. Chem. Chem. Phys.* **2006**, *8*, 3172.
(40) Bhatta, R. S.; Yimer, Y. Y. *Electron. J. Theor. Chem.* **2012**, *995*, 36.
(41) Breneman, C. M.; Wiberg, K. B. *J. Comput. Chem.* **1990**, *11*, 361.
(42) Ponder, J. W. *TINKER: Software Tools for Molecular Design*, 3.9 ed; Washington University School of Medicine: Saint Louis, MO, 2014.
(43) Gennes, P. G. D. *The Physics of Liquid Crystals*; Clarendon Press: Oxford, 1974.
(44) Marsh, H. S.; Jankowski, E.; Jayaraman, A. *Macromolecules* **2014**, *47*, 2736.
(45) Nguyen, T.-Q.; Yee, R. Y.; Schwartz, B. J. *J. Photochem. Photobiol., A* **2001**, *144*, 21.
(46) Wang, D.; Yuan, Y.; Mardiyati, Y.; Bubeck, C.; Koynov, K. *Macromolecules* **2013**, *46*, 6217.
(47) Huser, T.; Yan, M.; Rothberg, L. J. *Proc. Natl. Acad. Sci. U.S.A.* **2000**, *97*, 11187.
(48) Johnson, C. E.; Boucher, D. S. *J. Polym. Sci., Part B: Polym. Phys.* **2014**, *52*, 526.
(49) Hwang, I.; Scholes, G. D. *Chem. Mater.* **2011**, *23*, 610.
(50) Olivares-Amaya, R.; Amador-Bedolla, C.; Hachmann, J.; Atahan-Evrenk, S.; Sánchez-Carrera, R. S.; Vogt, L.; Aspuru-Guzik, A. *Energy Environ. Sci.* **2011**, *4*, 4849.
(51) Kanal, I. Y.; Owens, S. G.; Bechtel, J. S.; Hutchison, G. R. *J. Phys. Chem. Lett.* **2013**, *4*, 1613.
(52) Spano, F. C. *Acc. Chem. Res.* **2010**, *43*, 429.
(53) Bolinger, J. C.; Traub, M. C.; Brazard, J.; Adachi, T.; Barbara, P. F.; Vanden Bout, D. A. *Acc. Chem. Res.* **2012**, *45*, 1992.
(54) Peteanu, L. A.; Sherwood, G. A.; Werner, J. H.; Shreve, A. P.; Smith, T. M.; Wildeman, J. *J. Phys. Chem. C* **2011**, *115*, 15607.
(55) Jakubiak, R.; Collison, C. J.; Wan, W. C.; Rothberg, L. J.; Hsieh, B. R. *J. Phys. Chem. A* **1999**, *103*, 2394.
(56) Yamamoto, T.; Lee, B.-L.; Kokubo, H.; Kishida, H.; Hirota, K.; Wakabayashi, T.; Okamoto, H. *Macromol. Rapid Commun.* **2003**, *24*, 440.
(57) Li, Y.; Sonar, P.; Murphy, L.; Hong, W. *Energy Environ. Sci.* **2013**, *6*, 1684.
(58) Son, H. J.; Wang, W.; Xu, T.; Liang, Y.; Wu, Y.; Li, G.; Yu, L. *J. Am. Chem. Soc.* **2011**, *133*, 1885.
(59) Hammond, M. R.; Kline, R. J.; Herzing, A. A.; Richter, L. J.; Germack, D. S.; Ro, H.-W.; Soles, C. L.; Fischer, D. A.; Xu, T.; Yu, L.; Toney, M. F.; DeLongchamp, D. M. *ACS Nano* **2011**, *5*, 8248.
(60) Huo, M.-M.; Liang, R.; Xing, Y.-D.; Hu, R.; Zhao, N.-J.; Zhang, W.; Fu, L.-M.; Ai, X.-C.; Zhang, J.-P.; Hou, J.-H. *J. Chem. Phys.* **2013**, *139*, 124904.
(61) Grozema, F. C.; van Duijnen, P. T.; Berlin, Y. A.; Ratner, M. A.; Siebbeles, L. D. A. *J. Phys. Chem. B* **2002**, *106*, 7791.
(62) Kumar, R.; Goswami, M.; Sumpter, B. G.; Novikov, V. N.; Sokolov, A. P. *Phys. Chem. Chem. Phys.* **2013**, *15*, 4604.
(63) Carbone, P.; Troisi, A. *J. Phys. Chem. Lett.* **2014**, *5*, 2637.
(64) Venkateshvaran, D.; Nikolka, M.; Sadhanala, A.; Lemaur, V.; Zelazny, M.; Kepa, M.; Hurhangee, M.; Kronemeijer, A. J.; Pecunia, V.; Nasrallah, I.; Romanov, I.; Broch, K.; McCulloch, I.; Emin, D.; Olivier, Y.; Cornil, J.; Beljonne, D.; Sirringhaus, H. *Nature* **2014**, *515*, 384.
(65) Kim, B.-G.; Jeong, E. J.; Chung, J. W.; Seo, S.; Koo, B.; Kim, J. *Nat. Mater.* **2013**, *12*, 659.
(66) Park, Y. D.; Park, J. K.; Seo, J. H.; Yuen, J. D.; Lee, W. H.; Cho, K.; Bazan, G. C. *Adv. Energy Mater.* **2011**, *1*, 63.
(67) Padinger, F.; Rittberger, R. s.; Sariciftci, N. s. *Adv. Funct. Mater.* **2003**, *13*, 85.
(68) Peet, J.; Kim, J. Y.; Coates, N. E.; Ma, W. L.; Moses, D.; Heeger, A. J.; Bazan, G. C. *Nat. Mater.* **2007**, *6*, 497.
(69) Flory, P. J. *Principles of Polymer Chemistry*; Cornell: Ithaca, NY, 1953.
(70) Burgués-Ceballos, I.; Machui, F.; Min, J.; Ameri, T.; Voigt, M. M.; Luponosov, Y. N.; Ponomarenko, S. A.; Lacharmoise, P. D.; Campoy-Quiles, M.; Brabec, C. J. *Adv. Funct. Mater.* **2014**, *24*, 1449.
(71) Machui, F.; Abbott, S.; Waller, D.; Koppe, M.; Brabec, C. J. *Macromol. Chem. Phys.* **2011**, *212*, 2159.
(72) Hansen, C. M. *Prog. Org. Coat.* **2004**, *51*, 77.
(73) Jackson, N. E.; Chen, L. X.; Ratner, M. A. *J. Phys. Chem. B* **2014**, *118*, 5194.

DOI: 10.1021/jacs.5b00493
J. Am. Chem. Soc. 2015, 137, 6254−6262